PASSIVE DYNAMIC WALKER KINEMATICS REPORT

Group 5: Aaruni Arora, Joshua Bateman, Emmanuelle Ghaleb, Khalid Jama, Alexander Timms

INTRODUCTION

Passive Dynamic Walking (PDW) offers invaluable insight into the biomechanics of bipedal locomotion, by exploring how legged mechanisms can achieve stable gait cycles, with minimal input and no active control. These models were originally pioneered by McGeer in 1990, demonstrating that stable human-like walking can be achieved from simplistic mechanical interactions with the environment, relying solely on gravitational energy to sustain motion [1].

Our PDW model follows the implementation of Garcia et Al. and consists of two rigid, massless legs connected by a frictionless hinge at the hip, where the primary source of inertia is contained [2]. The model relies on the gravitational energy from the sloped surface to fuel its double-pendulum-like movement. This energy facilitates the model to swing one leg freely forward while keeping the other in contact with the ground, when this leg makes impact with the ground (heel strike) it becomes the stance leg [3]. The previous stance leg then lifts off the ground and transitions into the swing leg. This gait cycle continues and can be self-sustaining under the right conditions (e.g. no energy losses), allowing the model to continuously walk down the slope indefinitely without additional control.

This study focuses on digitising and analysing the best PDW performance recorded within our group. Using kinematic analysis, we investigate the stability and variability of passive walking episodes. Specifically, we examine how step consistency, stance angles, inter-leg angles, and energy fluctuations compare with theoretical predictions from simulation models. By processing multiple walking trials, we aim to identify trends and deviations that provide deeper insight into passive gait mechanics. Specifically, we will be investigating the stance angle from $3° - 12°$ and the inter-leg angel from $34° - 46°$ at a 4° slope.

1 OBJECTIVES

The primary object of the study are as follows:

1.1 Digitisation and Performance Evaluation

Identify and digitise the most stable walking trial, between the specified angles at a slope of 4°. Ensuring the step consistency and repeatability are accurately represented in the digitised data.

1.2 Tuning Map Visualisations

Develop a comprehensive tuning map to represent PDW's performance during experimentation by conducting multiple trials to mitigate against experimental error and ensure fair environmental conditions in each PDW experiment. Compare the experimental tuning map with the theoretical simulations conducted with MATLAB.

1.3 Kinematic and Dynamic Analysis

Analyse the stance and inter-leg angles over time to access gait stability of the walker. Use this information to construct state-space trajectories of the walker to identify the indicators of instability of the model. Estimate the centre of mass (CoM) trajectories and derive mechanical quantities. Compare these with the theoretical expectations to identify mistakes of our model.

1.4 Energy Analysis

De-trend the potential energy (PE) fluctuations and compare with the kinetic energy (KE), to identify the differences in energy dissipation and dynamics in comparison to the MATLAB-based PDW simulations.

2 METHODS

2.1 Walker Assembly

Constructing a functioning and reliable walker was crucial for data collection. We built a total of 4 walkers following the *PDW Assembly Guide* [4] provided. Through preliminary experimentation with walker 3 we realised that we need additional markers and higher resolution to aid with walker-tracking for the analysis. Thus, we used walker 4, with multiple white and black markers to aid in our final experimentations.

2.2 PDW Testing

We tested 16 different input parameters for the walker at a ramp angle of 4°. Each input parameter was tested 5 times to find the maximum number of steps. The initial stance angle was varied from 3° to 12° in increments of 3°, and initial inter-leg angle was varied from 34° to 46° in increments of 4°. Before testing, we ran a MATLAB simulation to determine the trends of our input parameters. We assigned roles according to recommendations in the course *Unit 2 instructions* [5]: one student sets up the walker angles, a second handles the release, a third records the experiments, and a fourth makes notes and handles the running of experiments.

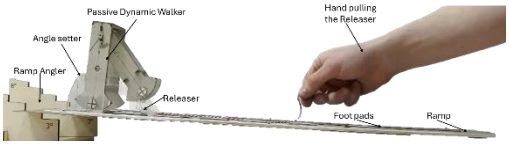

Figure 1. Picture of the experimental setup

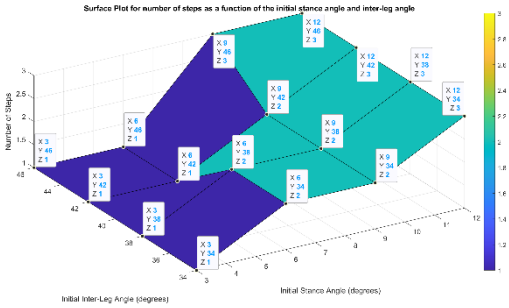

Figure 2. MATLAB simulation for number of steps (Z) for various of initial inter-leg (Y) and stance angles (X).

We systematically ran through the input parameters, starting with the lowest initial inter-leg angle and iterating through the stance angles before moving onto the next inter-leg angle. We conducted a few trial runs for each set of parameters to ensure the stepping pads are placed optimally before proceeding with the 5 trials.

2.3 MATLAB Analysis

We used the *DLTdv8* MATLAB app to digitise and analyse our best walker recording (inter-leg angle=42). We tracked the desired parts of the walker on the app using the semi-auto and manual modes, which can be seen in Table 1 and Figure 3. We then exported the position vectors for all points for data analysis in Python.

Table 1. List of tracking points positioned on the walker

Point	Location	Use
1	Tip of arrow pointer	Calculate the angle of the inner leg referenced with the outer
2	Rod centre	Hip joint, reference point for all calculations
3	CoM of the outer leg	Tracking CoM for the outer leg system
4	CoM of the inner leg	Tracking CoM for the inner leg system
5	Point mass on outer leg	Useful for calculating stance and inter-leg angle
6	Point mass on inner leg	Useful for calculating stance and inter-leg angle

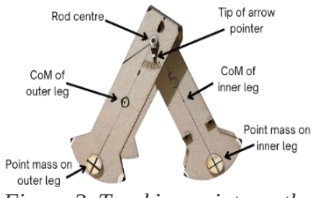

Figure 3. Tracking points on the

We first converted from pixels to meters by taking the average of ramp length, walker width and support length. The inter-leg, φ and stance, θ, angles were calculated using Equation (1) and **Error! Reference source not found.** for gait analysis.

$$\varphi = arctan\left(\frac{(BA_x \times BC_y) - (BA_y \times BC_x)}{(BA_x \times BC_x) + (BA_y \times BC_y)}\right) \quad (1)$$

In Equation (1)$\varphi = arctan\left(\frac{(BA_x \times BC_y) - (BA_y \times BC_x)}{(BA_x \times BC_x) + (BA_y \times BC_y)}\right)$ we substituted B with the rod positions, A with the position of the arrow pointer tip, and C with the outer leg mass positions to calculate φ. For θ, we first used heel strikes to switch the stance leg between outer to inner leg point mass Here, A is the stance leg, B the rod position and C a point on the line perpendicular to the ramp.

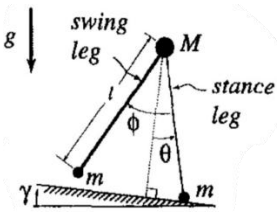

Figure 4. Mathematical derivations of inter-leg angle and stance angle.

The CoM was manually found through suspension method and points were marked on the inner and outer leg for tracking. As CoM changes as the walker is walking, it was calculated by weighted positional values of points 2, 3 and 4 (Table 1). The position data was passed through a 2nd order low-pass Butterworth filter with a cut-off frequency of 12.5Hz [2]. Potential energy (de-trended) and be kinetic energy could then be calculated using $PE = mgh$ and $KE = \frac{1}{2}mv^2$ where $h = CoM_y - tan(slope) * CoM_x$ and $v^2 = \sqrt{v_x^2 + v_y^2}$ [6].

3 RESULTS & DISCUSSION

3.1 Tuning map and Heat-map

3.1.1 Tuning Map

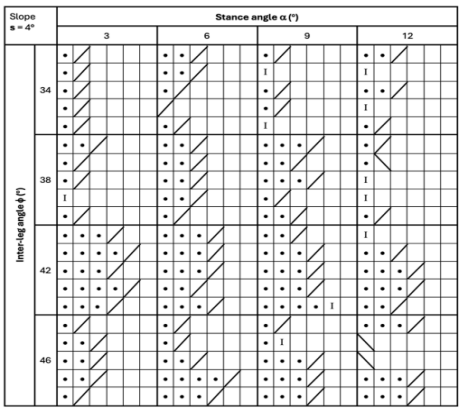

Figure 5. Tuning Map of PDW for different Initial Inter-Leg and Stance Angles.

The tuning map in Figure 5 shows the relationship between stance angles (α) and inter-leg angles (ϕ) at a slope of 4°. Each cell relates to the walker's behaviour during a step of a trial at a specific combination of angles. Forward falls (/) are most frequent when the stance angle is small, while backward falls (\) occur for the cases where the PDW immediately falls due to inconsistent initial pulling or when the stance angle is too large. Successful steps (●) are concentrated in regions with mid-range stance and high inter-leg angles, indicating optimal conditions for stable, periodic walking. Cells with no steps but no falls (I) represent minor stability zones where the walker gets stuck, unable to move forward due to a wide inter-leg angle or insufficient momentum. Instability increases at extreme stance and inter-leg angles, resulting in more frequent falls. The results are prone to variation due experimental errors, brought about by incorrect setup or misconfigured walkers. Thus, we take an average of 5 trials for our data analysis.

3.1.2 Heat-map

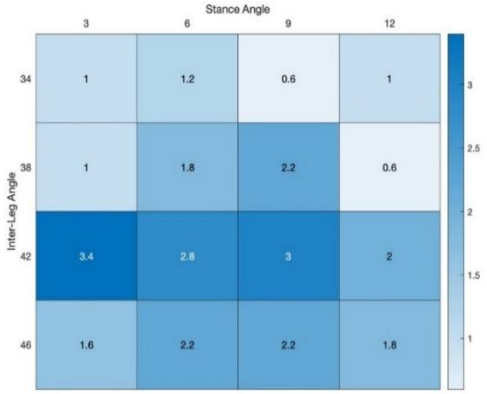

Figure 6. Heatmap for PDW's step count as a function of initial stance angle and initial inter-leg angle in real-world (based on 3.1.1).

Figure 2 and Figure 6 respectively compare the simulated and real-world walker's step count at various initial stance and inter-leg angles. The differences in step count highlight discrepancies due to modelling assumptions, surface interactions, and measurement limitations. The simulation assumes idealised conditions, while real-world trials face mechanical imperfections like joint stiffness, friction, and tracking errors. Notably, the simulated walker performed far worse at low stance angles (3°–6°) in comparison to the real-world walker that saw some success for a low stance angle (3°) and a high inter-leg angle (42°–46°). Another discrepancy is that in the simulated data, a low inter-leg angle (34°) combined with a high stance angle (9°–12°) resulted in a comparatively high number of steps, whereas in the real-world data, step counts remained consistently lower. This misalignment is also due to experimental error, as the real-world step averages were skewed downward by failed walker trials.

3.2 Performance video analysis

The performance and stability of the PDW can be analysed by plotting the inter-leg and stance angles as a function of time or steps (non-dimensional time) for an initial inter-leg angle of 42° and stance angle of 3°.

3.2.1 Inter-leg angle variation

The plots in Figure 7 capture the kinematic behaviour of the PDW as it walks for four steps before falling. Each step is characterised by an inter-leg angle local extremity, where a local maximum indicates a step with the inner leg in air and a local minimum indicates a step with the outer leg in the air. This discrimination can be normalised by plotting the absolute value of the angle where 0° indicates the legs crossing and local maximum indicates a stride. This will be done for the stance angle in Figure 8 as well.

At 0.4s, the beginning of a step, the inter leg angles drop dramatically from 42° to -23°. However, this peak-to-peak magnitude shows an exponential decay over time, resulting in final oscillations under 10° when the PDW falls. This reduction of maximum absolute magnitude is a result of energy dissipation due to friction from the pads in most cases. The momentum gain and loss can be seen by the difference in the length of time separating the zero-crossing points, indicating near alignment of the legs: the period of each step first increases to 0.6s by the third step and then starts falling from the fourth step to 0.4s. After 1.5s, a chaotic pattern emerges

as the walker loses stability and balance, developing an excessively narrow inter-leg angle that prevents continued motion, leading to a fall onto the ramp. The fluctuations dissipate, converging to 0° at 2.3s when the walker becomes stationary.

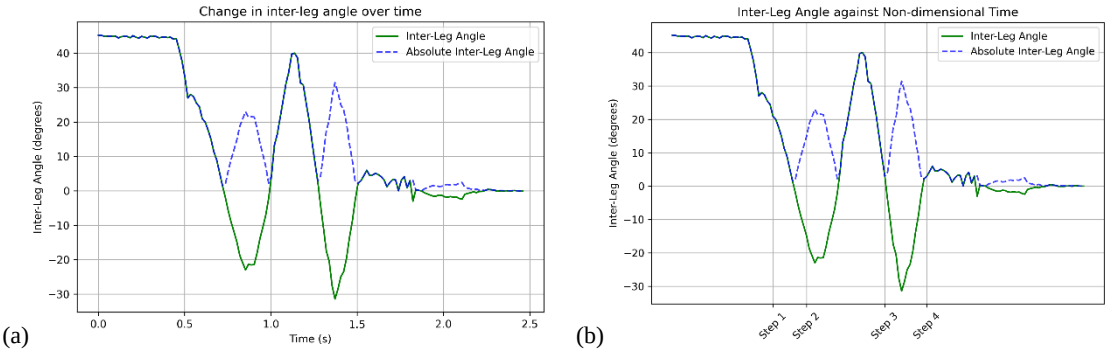

Figure 7. PDW inter-leg angle as a function of (a) time and (b) non-dimensional time

3.2.2 Stance angle variation

In Figure 8, the absolute stance angle increases from 3°, as the PDW makes its first step at 0.4s. The rhythmic oscillations show a controlled gait throughout the trial. One clear stance angle cycle can be seen during step 3 from 0.7s to 1.4s. During this phase, the stance angle oscillates to a minimum at 0.85s and the inter-leg angle reduces to ~4° at 0.9s as the PDW switches stance legs. After this the stance and inter leg angles rise again as the walker progresses forward. A spike in the stance angle is detected at 1.8s, corresponding to the PDW falling perpendicular to the floor. This 90° spike occurs because the stance angle is measured relative to the line normal to the ramp. This is also why there are no fluctuations observed here, as the PDW falls, as compared to the inter-leg angle.

Figure 9 further examines the inter-leg angle as a function of stance angle across multiple steps.

- Step 1: The stance angle follows a smooth trajectory, indicating stability and effective energy utilisation.
- Step 2: The trajectory becomes more erratic, with the stance angle showing larger deviations and oscillations, signalling increasing momentum.
- Step 3: Has the highest energy with the longest period and an irregular state space trajectory. The pattern observed is also due to the interpolation between stance legs as the inner leg gets hidden by the outer leg, reducing the quality of the available data for analysis.
- Step 4: Has a similar trajectory to step 2 as the energy and momentum decreases and the walker faces challenges in maintaining balance during heel strikes
- Step 5 (falling): Mimicking the high energy, irregular pattern of step 3, this step highlights the walker's ability to sustain controlled motion during the other steps.

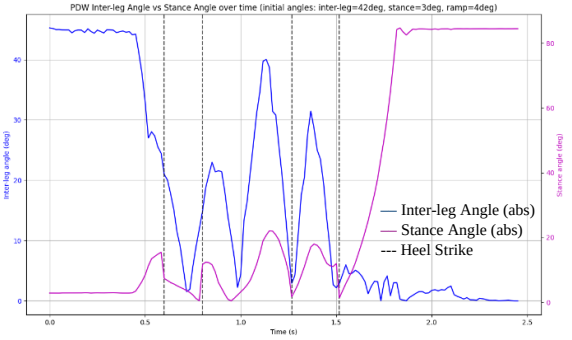

Figure 8. Absolute values of Inter-leg Angle vs Stance Angle over time with each step annotated with black dotted line.

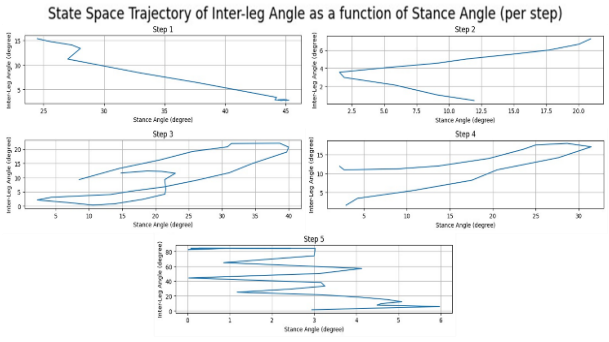

Figure 9. State Space Trajectory of absolute values of Inter-leg Angle as a function of absolute values of Stance Angle per step.

3.2.3 Energy analysis

The trajectory of the Centre of Mass (CoM) was measured over time and plotted in Figure 10. CoM values are initially stable, with x increasing linearly and y decreasing as the walker moves down the ramp; it then re-stabilises after the walker falls. The fluctuations seen in the y trajectory are due to

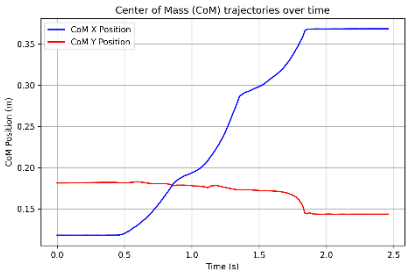

Figure 10. Trajectory of the CoM over time.

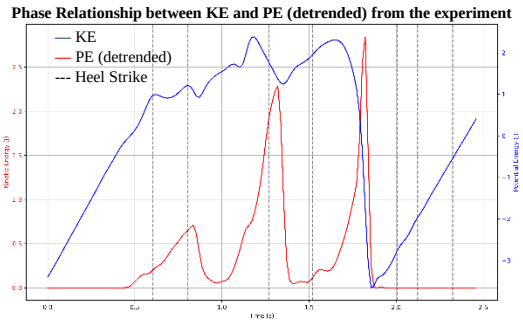

Figure 11. Phase relationship between KE and PE (Detrended) of the PDW over time

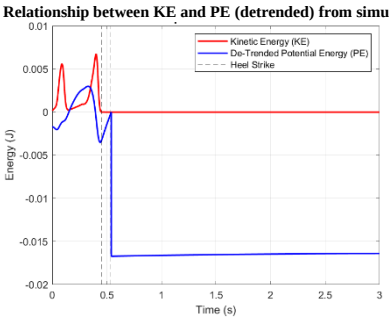

Figure 12. Phase relationship between KE and PE (Detrended) of the PDW simulation over time

the heel strikes and the downward linear trend is due to the ramp slope, which is why we de-trended the potential energy plot.

The de-trended potential energy (PE) and kinetic energy (KE) were calculated with equations from Section 2.3 and plotted as functions of time in Figure 11. The plot reveals distinct energy exchanges during the walking motion with the KE dropping as the PE rises and vice-versa. This is observed in both the simulation, where the PDW only achieves 1 step, and the experiment, where it achieves 4 steps. This could be due to additional energy supplied when pulling the support instead of simply letting it fall in the simulation. As time progresses, irregularities in the energy profiles become apparent especially in the experiment graph where energy loss is more prominent [7].

In both the simulation and the experiment, when both legs are in contact with the ground, the KE reaches 0, representing the transition between steps when the walker is momentarily stationary. Following this, as the model switches to a single-leg support, the KE increases and peaks right after the stance at the beginning of a step. This indicates a transition state where the CoM goes from behind the contact point to in front, causing the weight to shift and therefore falls forward eventually changing the weight-supporting leg, which is what triggers the motion. The potential energy's cycle is complementary to the KE's: when both legs are in contact with the floor, the PE peaks and falls as the weight shifts. In the simulation, these fluctuations appear smoother and more periodic, with stable gait cycles, as the plot is based on more data points and is not dependent on human tracking. However, due to energy loss, friction against the pads and low momentum, both models fall. This fall is indicated by a spike caused by the energy increase of the fall followed by a drop in KE and later PE at 1.9s, when the walker collapses as it destabilises and loses balance.

3.3 Evaluation

The results exhibit deviations from theoretical expectations due to human error and measurement limitations: 11 points were manually tracked on *DLTdv8*, based on assumptions and estimated marker positions, introducing potential inaccuracies. Additionally, the tracking precision was constrained by pixel resolution and low frame rate, but this can be improved with higher-resolution imaging, finer markers, and automated tracking. Further, inconsistencies in walker performance, such as missing or tripping on pads, can be corrected by conducting more pre-liminary trials and standardising the initial pulling mechanism for reproducibility.

4 CONCLUSION

This study analysed Passive Dynamic Walking through experimental trials and simulations, assessing gait stability, energy transitions, and deviations from theoretical predictions. While real-world trials showed greater stability at certain angles compared to simulations, inconsistencies arose due to frictional losses, tracking inaccuracies, and walker misalignment. Energy analysis confirmed expected oscillatory behaviour between kinetic and potential energy, though experimental data exhibited irregularities due to dissipation effects. Future improvements should focus on higher-resolution imaging, automated tracking, and standardized release mechanisms to enhance accuracy and reproducibility. Overall, this study demonstrates the feasibility of PDW, providing insights into energy-efficient bipedal locomotion and informing future biomechanical and robotic applications.

REFERENCES

[1] T. McGeer, 'Passive Dynamic Walking', *Int J Rob Res*, vol. 9, no. 2, pp. 62–82, Apr. 1990, doi: 10.1177/027836499000900206.

[2] M. Garcia, A. Chatterjee, A. Ruina, and M. Coleman, 'The Simplest Walking Model: Stability, Complexity, and Scaling', *J Biomech Eng*, vol. 120, no. 2, pp. 281–288, Apr. 1998, doi: 10.1115/1.2798313.

[3] F. Asano, M. Yamakita, N. Kamamichi, and Z. W. Luo, 'A novel gait generation for biped walking robots based on mechanical energy constraint', *IEEE Transactions on Robotics and Automation*, vol. 20, no. 3, pp. 565–573, Jun. 2004, doi: 10.1109/TRA.2004.824685.

[4] Dr Huai-Ti Lin, 'ALBiR PDW Assembly Guide', 2023.

[5] H.-T. Lin, 'ALBiR Unit 2: Passive Dynamic Walker', 2025. Accessed: Feb. 03, 2025. [Online]. Available: https://biomech.web.unc.edu/dltdv/

[6] A. D. Kuo and J. M. Donelan, 'Dynamic Principles of Gait and Their Clinical Implications', *Phys Ther*, vol. 90, no. 2, p. 157, Feb. 2010, doi: 10.2522/PTJ.20090125.

[7] R. Tedrake, T. W. Zhang, M.-F. Fong, and H. S. Seung, 'Actuating a Simple 3D Passive Dynamic Walker'.